NASA/TM—2011-217282

Buckling and Vibration of Fiber Reinforced Composite Plates With Nanofiber Reinforced Matrices

Christos C. Chamis and Pappu L.N. Murthy
Glenn Research Center, Cleveland, Ohio

December 2011

NASA STI Program . . . in Profile

Since its founding, NASA has been dedicated to the advancement of aeronautics and space science. The NASA Scientific and Technical Information (STI) program plays a key part in helping NASA maintain this important role.

The NASA STI Program operates under the auspices of the Agency Chief Information Officer. It collects, organizes, provides for archiving, and disseminates NASA's STI. The NASA STI program provides access to the NASA Aeronautics and Space Database and its public interface, the NASA Technical Reports Server, thus providing one of the largest collections of aeronautical and space science STI in the world. Results are published in both non-NASA channels and by NASA in the NASA STI Report Series, which includes the following report types:

- TECHNICAL PUBLICATION. Reports of completed research or a major significant phase of research that present the results of NASA programs and include extensive data or theoretical analysis. Includes compilations of significant scientific and technical data and information deemed to be of continuing reference value. NASA counterpart of peer-reviewed formal professional papers but has less stringent limitations on manuscript length and extent of graphic presentations.

- TECHNICAL MEMORANDUM. Scientific and technical findings that are preliminary or of specialized interest, e.g., quick release reports, working papers, and bibliographies that contain minimal annotation. Does not contain extensive analysis.

- CONTRACTOR REPORT. Scientific and technical findings by NASA-sponsored contractors and grantees.

- CONFERENCE PUBLICATION. Collected papers from scientific and technical conferences, symposia, seminars, or other meetings sponsored or cosponsored by NASA.

- SPECIAL PUBLICATION. Scientific, technical, or historical information from NASA programs, projects, and missions, often concerned with subjects having substantial public interest.

- TECHNICAL TRANSLATION. English-language translations of foreign scientific and technical material pertinent to NASA's mission.

Specialized services also include creating custom thesauri, building customized databases, organizing and publishing research results.

For more information about the NASA STI program, see the following:

- Access the NASA STI program home page at *http://www.sti.nasa.gov*

- E-mail your question via the Internet to *help@sti.nasa.gov*

- Fax your question to the NASA STI Help Desk at 443–757–5803

- Telephone the NASA STI Help Desk at 443–757–5802

- Write to:
  NASA Center for AeroSpace Information (CASI)
  7115 Standard Drive
  Hanover, MD 21076–1320

NASA/TM—2011-217282

Buckling and Vibration of Fiber Reinforced Composite Plates With Nanofiber Reinforced Matrices

Christos C. Chamis and Pappu L.N. Murthy
Glenn Research Center, Cleveland, Ohio

National Aeronautics and
Space Administration

Glenn Research Center
Cleveland, Ohio 44135

December 2011

This report contains preliminary findings, subject to revision as analysis proceeds.

This work was sponsored by the Fundamental Aeronautics Program at the NASA Glenn Research Center.

Level of Review: This material has been technically reviewed by technical management.

Available from

NASA Center for Aerospace Information
7115 Standard Drive
Hanover, MD 21076–1320

National Technical Information Service
5301 Shawnee Road
Alexandria, VA 22312

Available electronically at http://www.sti.nasa.gov

Buckling and Vibration of Fiber Reinforced Composite Plates With Nanofiber Reinforced Matrices

Christos C. Chamis and Pappu L.N. Murthy
National Aeronautics and Space Administration
Glenn Research Center
Cleveland, Ohio 44135

Abstract

Anisotropic composite plates were evaluated with nanofiber reinforced matrices (NFRM). The nanofiber reinforcement volumes ratio in the matrix was 0.01. The plate dimensions were 20 by 10 by 1.0 in. (508 by 254 by 25.4 mm). Seven different loading condition cases were evaluated for buckling: three for uniaxial loading, three for pairs of combined loading, and one with three combined loadings. The anisotropy arose from the unidirectional plates having been at 30° from the structural axis. The anisotropy had a full 6 by 6 rigidities matrix which were satisfied and solved by a Galerkin buckling algorithm. For vibration the same conditions were used with the applied cods about a small fraction of the buckling loads. The buckling and vibration results showed that the NFRM plates increased about twice those with conventional matrix.

Introduction

Considerable research activities in nanocomposites have been actively pursued recently. One aspect of this research is on nanofiber reinforced matrices (NFRM) which can subsequently be used as matrices in conventional reinforced fiber composites. As of to date, the buckling of composite plates with NFRM has not been investigated yet. This is the objective of the present paper, to use a commercial composites loaded at 30° (Fig.1) from the material axis for seven different cases. The results are compared with fiber composite without the NFRM that is an AS/IMHS (AS graphite fiber/intermediate modulus high strength matrix) for all the loading conditions and for both buckling and vibration. Because the 30° off-axis composite has a full 6×6 bending stiffness matrix, a Galerkin algorithm is used to evaluate the buckling factor. The bending stiffness required for the buckling of off-axis loaded anisotropic composite were generated by the in-house integrated computer code in composite mechanics. The comparison of results without and with the NFRM show about twice the buckling factor for all loading conditions with only 1 percent of nanofiber reinforced matrix. Results are presented for the buckling factor mode and its corresponding buckling factor for each loading condition. The graphical results shown will be for the type of loading condition, the 3–D buckling factor mode shape, a contour plot of the buckling factor mode and a convergence plot of the buckling algorithm. One interesting result is that the shear buckling factor does not converge and requires a tiny small loading in one or both structural axes to enhance the convergence.

The theory was developed when the first author was a graduate student at Case Western Reserve University and it is described in Reference 1. The application to the anisotropic plates was performed when he started working at NASA Lewis Research Center (now Glenn Research Center) Reference 2. The programming details source code and several sample cases are in the appendices of Reference 2. The brief description of the theoretical background is from Reference 2 also.

The underlying theory for buckling factors of anisotropic plates is described in References 1 and 2 with pertinent discussions in References 3 to 5. Briefly, this theory consists of expressing the potential energy of plate in terms of displacement variables. Taking the variation of the potential energy function yields the field equation and the corresponding boundary conditions. The resulting system then is solved by the assumed mode technique in conjunction with the Galerkin method (Fig. 2).

The equation resulting after the variation of the energy function is

$$\int_0^a \int_0^b \Big[D_{11}w_{,xxxx} + 2(D_{12} + 2D_{33})\, w_{,xxyy} + D_{22}w_{,yyyy} + 4D_{13}w_{,xyxx} + 4D_{23}w_{,xyyy} - \left(\overline{N}_X w_{,xx} + 2\overline{N}_{xy} w_{,xy} + N_y w_{,yy}\right)\Big]\, \delta w\, dy\, dx + \int_0^b \Big(D_{11}w_{,xx} + D_{12}w_{,yy} + 2D_{13}w_{,xy}\Big|_0^a \delta w_{,x}\, dy + \int_0^a \Big(D_{21}w_{,xx} + D_{22}w_{,yy} + 2D_{23}w_{,xy}\Big|_0^b \delta w_{,y} dx = 0 \tag{1}$$

(The notation is defined in Appendix A of Reference 2). The area integral represents the field equation, and the line integrals represent the boundary conditions.

The assumed buckling factor mode described in Reference 2 is represented by a Fourier double sine series. This mode satisfies the imposed boundary conditions, but it does not satisfy the natural boundary conditions if the material and structural axes do not coincide. However, the mode is forced to satisfy the natural boundary conditions approximately through the Galerkin method as discussed in Reference 2.

Substituting the assumed mode in Equation (1), applying the Galerkin method, and carrying out the algebra result in a set of linear equations for buckling

$$[K]\ \{w\} = \lambda\, [L]\ \{w\} \tag{2}$$

and for vibration is

$$[M]\{\ddot{w}\} + [K - L]\, w = \lambda \{w\} \tag{3}$$

where K is the stiffness matrix, λ is the eigenvalue [L] is the loading matrix [M] is the mass matrix, $\{\ddot{w}\}$ is the acceleration and $\{w\}$ is the displacement vector. This system is coupled for either a combination of shear and normal loads and/or noncoincident material and structural axes.

The eigenvalue problem is solved by using the Power method, which is a highly effective iterative numerical technique in seeking the largest eigenvalue of the system. The indicial equations which were used to generate this system and the Power method are given in Appendix B of Reference 2 in outline form.

The source code has been reprogrammed by Dr. Murthy in Metlab. The results for both presented subsequently are from the Metlab reprogrammed. There are two portions to the results: (1) is the simulation of the NFRM which is performed by a composite mechanics code ICAN/JAVA in order to obtain the nanofiber reinforcement in the matrix and (2) using the NFRM in the mechanics computer code again to simulate the effects of the reinforced matrix in the buckling and vibration behavior of the composite plate for different combination of loads.

The nanofiber reinforced matrix (NFRM) is simulated by using the continuous solid nanofiber properties shown in Table 1 in an intermediate modules high strength matrix in Table 2 assuming a quasi isotropic fiber arrangement. The properties of this lay-up arrangement are shown in Table 3. Next, the conventional fiber in Table 4 was used with the NFRM to obtain the bending rigidities shown in Table 5.

Buckling Results and Discussion

The composite plate shown in Figure 1 was selected for the buckling evaluation. The fiber reinforcement was 0.6 volume ration in a NFRM. The bending rigidities shown in Table 5 were transformed to 30° from the structural x-axis to obtain the anisotropic composite plate. The transformed rigidities were input into the buckling routine with the plate geometry (20×10×1.0) length, width, thickness and the results were obtained for seven different cases of combined in plane loads. For convenience all the inplane loads were assumed to be of equal magnitude. Two different buckling results are shown for conventional matrix Table 6 and for NFRM Table 7.

The buckling factor conditions indicated in each table with a check mark. Note that the structural axis has only one check mark in the first column. The y axis has one check mark in the second column. The x-y loading has a check mark in the third column combined load cases leave check marks in the appropriate column to indicate the combined loading.

Comparing the buckling results of the two tables it is seen that the plates with the NFRM is about twice of the conventional matrix.

Buckling Factor Mode Shapes

The buckling factor mode shapes of anisotropic plates is very interesting. In this evaluation buckling factor mode shapes were evaluated for each loading condition that means there are seven charts of buckling factor mode shapen. Each chart has four parts in it. The top left (a) is a contour part of the modal shape. The upper left (b) is a 3–D view of the buckling factor mode shape. The lower left (c) is a buckling factor convergence plot. The lower right (d) is a box with the following information in it: first line loading conditioning, second line, load axis; third line the buckling factor of that case.

Part (a) in Figure 3(a) depicts the contour plot of the buckling factor mode shape for buckling factor in the x direction. Part (b) depicts a 3–D presentation of the buckling factor mode shape. Part (c) depicts the buckling factor convergence in 8 interactions. Part (d) is the box with all the information of the mode shape. Note that the plate buckled in two modes. The buckling factor is 3673 lb (163.38 kN).

Figure 4 depicts analogous information or the buckling factor in the transverse direction. Part (a) is the contour plot; part (b) is the 3–D view of the mode shape; part (c) is the convergence plot in 6 interactions and part (d) is the buckling information box. The buckling factor is 1097 lb (48.79 kN).

Figure 5 depicts similar information of the shear load buckling shape. Note that this mode shape symmetric about the material axis 30° from the x axis. Note that buckling factor converged in 7 interactions. Note also that the very small load of 1 lb (4.448 N) in the x- and y-axis as was previous explained. The buckling factor is 2220 lb (98.75 kN).

Figure 6 depicts the buckling factor mode shape of bi-axial combined loads. Note that this contour plot depicts a symmetric mode shape about the material axes also. Note also the buckling factor converged in 6 iterations as well. The buckling factor is 875 lb (3.892 kN).

Figure 7 is the buckling factor mode shape of combined buckling factor axial and shear. The contour plot of this mode shape also is symmetric about the material axis. Note the buckling factor converged in 7 iterations. The buckling factor is 1520 lb (6.761 kN).

Figure 8 is the buckling factor mode shape of a y-axis and shear load. As was the case previously the contour plot show symmetry about the material axis. The buckling factor converged in 8 iterations with a value of 808 lb (35.94 kN).

Figure 9 depicts the buckling factor mode shape of combined loads x, y, and xy. The buckling factor converged in 8 iterations to a value of 680 lb (30.25 kN).

Vibration Results and Discussion

The composite plate shown in Figure 1 was selected for the dynamic evaluation. The fiber reinforcement was 0.6 volume ration in a NFRM. The bending rigidities shown in Table 5 were transformed to 30° from the structural x-axis to obtain the anisotropic composite plate. The transformed rigidities were input into the frequency routine with the plate geometry (20×10×1.0) length, width, thickness and the results were obtained for seven different cases of combined in plane loads. For convenience all the inplane loads were assumed to be of equal magnitude. Two different frequency results are shown for conventional matrix Table 6 and for NFRM Table 7.

The vibration frequency evaluations indicated in each table with a check mark. Note that the structural axis has only one check mark in the first column. The y axis has one check mark in the second column. The x-y loading has a check mark in the third column combined load cases leave check marks in the appropriate column to indicate the combined loading.

Comparing the frequency results of the two tables it is seen that the plates with the NFRM is about 60-percent of the conventional matrix.

Vibration Frequencies Mode Shapes

The vibration frequencies mode shapes of anisotropic plates is very interesting. In this evaluation vibration frequencies mode shapes were evaluated for each loading case that means there are seven charts of vibration frequencies mode shapes. Each chart has four parts in it. The top is a counter part of the modal shapes. The center is a 3–D view of the buckling factor and the vibration frequencies mode shape. The lower part shows the angle of the anisotropy.

The top part in Figure 10 depicts the counter plot of the load factor and the vibration frequencies mode shape for load factor and frequency in the x direction. The center part is a 3–D mode shape. The lower part is the box with all the information of the mode shape. Note that the plate buckled in two modes. The load factor is 3673 lb (163.38 kN) and the frequency is 2005 Hz.

Figure 11 depicts analogous information of the load factor and the transverse direction and the corresponding frequency. The load factor is 1097 lb (48.79 kN) and the frequency is 1818 Hz.

Figure 12 depicts similar information of the shear load frequency shape of the load factor. This mode shape is symmetric about the material axis 30° from the x axis. Note that frequency converged. Note that the very small load of 1 lb (4.448 N) in the x and y axis as was previous explained. The load factor is 2220 lb (98.75 kN) and the frequency is 2245 Hz.

Figure 13 depicts the frequency mode shape of bi-axial combined loads. Note that this counter plot depicts a symmetric mode shape about the material axes also. The load factor is 875 lb (3.892 kN). The frequency is 1819 Hz.

Figure 14 is the load factor and frequency mode shape of combined loads axial and shear. The load factor counter plot shows symmetric about the material axis. The load factor is 1520 lb (6.761 kN) and the frequency is 2121 Hz.

Figure 15 is the load factor and frequency mode shape of a y-axis and shear load. As was the case previously, the counter plot show symmetry about the material axis. The frequency converged in 8 iterations with a value of load factor 808 lb (35.94 kN) and the frequency is 1909 Hz.

Figure 16 depicts the load factor and frequency mode shape of combined loads x, y, and xy. The load factor is 680 lb (30.25 kN) and the frequency is 1898 Hz.

Figure 17 shows the first six lowest frequencies of a square composite plate. Note that as the number of frequencies increases the mode shapes increase also.

Figure 18 is a similar graph of a rectangular anisotropic composite plate. Note that the two plates vibrate differently. For example, the four vibration modes occur in the fourth frequency modes in the rectangular plate whereas the four modes occur in the fifth vibration frequency mode in the square plate.

Figure 19 depicts the two lower modes as a function of load. Interesting to note that as the load increases both frequencies decrease with the first frequency decreasing at a faster rate at higher load.

Figure 20 is a graphical presentation of the orientation angle effects on the first frequency. Note that the frequency decreases nonlinearly at higher angles.

Figure 21 shows that the error decreases nonlinearly and at a slower rate as the number of terms in the Galerkin procedure increases.

Figure 22 shows the highly nonlinear effects of increasing load in the natural frequencies reaching zero at some load which corresponds to the buckling load. Note that the 45° curve reaches "zero" before the 60° curve. It also shows that at higher ages (>45°) the frequencies reach "zero" progressively.

Concluding Remarks

The concluding remarks of a buckling of anisotropic composite plates with NFRM are as follows. The nanofiber reinforcement has a major effect in the buckling factor. All the cases investigated for combined loads showed the same about twice benefit compared to conventional matrix. All buckling factor mode shape were single except the one loaded alone the structure x-axis which had double mode. All buckling factor mode contour plot showed symmetry about the matrix axis except the first case which showed symmetry about 45° to the structural x-axis. The shear loading only case required a small load in the two other orthogonal axes to expedite convergence. All buckling factor converged between 6 and 8 iterations. The buckling algorithm is very effective and its convergence is efficient. The simulation of the nanofiber reinforced matrix is also an effective means to obtain the influence of nanofibers in a matrix first and then combine the NFRF with the conventional fibers for other structural evaluations.

The concluding remarks of frequency response of anisotropic composite plates with NFRM are as follows. The nanofiber reinforcement has a major effect in the vibration frequencies. All the cases investigated for combined loads showed the same about 60 percent benefit compared to conventional matrix. All vibration frequencies of the mode shape are single. All vibration frequencies mode counter plot showed symmetry about the matrix axis except the first case which showed symmetry about 45° to the structural x-axis. The shear loading only case required a small load in the two other orthogonal axes to expedite convergence. All vibration frequencies converged between 6 and 8 iterations. The frequency algorithm is very effective and its convergence is efficient. The simulation of the nanofiber reinforced matrix is also an effective means to obtain the influence of nanofibers in a matrix first and then combine the NFRF with the conventional fibers for other structure evaluation loading. The loading has severe effects on the frequency. All frequencies derease nonlinearly with increasing load reaching "zero" at higher loads <45° and the "zero" load decreases at loads >45°. Frequencies decrease nonlinearly with increasing orientation angle. Mode shapes of square and rectangular plates differ at which frequency certain mode shapes will occur at a lower load.

References

1. Chamis, C.C.: Buckling of Anisotropic Composite Plates. J. Structural Div., ASCE, vol. 95, no. ST10, Oct. 1969, pp. 2119–2139.
2. Chamis, C.C.: Theoretical Buckling Loads of Boron/Aluminum and Graphite/Resis Fiber-Composite Anisotropic Plates. NASA TN D-6572, December 1971.
3. Wang, James T.-S.: On the Solution of Plates of Composite Materials. J. Composite Mat., vol. 3, July 1969, pp. 590–592.
4. Hsu, T.M.: Buckling of Anisotropic Plates, Discussion J. Structural Div., Am. Soc. Civil Eng., vol. 96, no. ST7, July 1970, p. 1604.
5. Chamis, C.C.: Buckling of Anisotropic Plates, Closure and Errata. J. Structural Div., Am. Soc. Civil Eng., vol. 97, no. ST3, Mar. 1971, p. 960.

TABLE 1.—NANOFIBER (TRIAL FIBER)
[TRIAL FIBER MODULUS 123M FOR SINGLE FIBER 3–D STRESS ANALYSIS.]

Description	Symbol	Value	Value in SI units
Number of fibers per end	Nf	100.0	100
Filament equivalent diameter	df	4.0×10^{-10} in.	1.016×10^{-8} mm
Weight density	Rhof	0.06 lb/in.^{3}	1.661×10^{-6} kg/mm^3
Normal moduli (11)	Ef11	1.0×10^9 psi	689.5×10^{10} Pa
Normal moduli (22)	Ef22	41.0×10^7 psi	282.7×10^{10} Pa
Poisson's ratio (12)	Nuf12	0.2 non-dim.	0.2 non-dim.
Poisson's ratio (23)	Nuf23	0.35 non-dim.	0.35 non-dim.
Shear moduli (12)	Gf12	2.0×10^7 psi	13.79×10^{10} Pa
Shear moduli (23)	Gf23	1.5×10^7 psi	10.34×10^{10} Pa
Thermal expansion coefficient (11)	Alfaf11	-6.0×10^{-8} in./in./°F	-10.8×10^{-8} /°C
Thermal expansion coefficient (22)	Alfaf22	6.0×10^{-6} in./in./°F	10.8×10^{-6} /°C
Heat conductivity (11)	Kf11	400.0 BTU/hr/in./°F	8.3075 W/mm/°C
Heat conductivity (12)	Kf12	40.0 BTU/hr/in./°F	0.83075 W/mm/°C
Heat capacity	Cf	0.17 BTU/lb/°F	712.3 J/kg/°C
Dielectric strength (11)	Kef11	0.0 V/in.	0.0 V/mm
Dielectric strength (22)	Kef22	0.0 V/in.	0.0 V/mm
Dielectric constant (11)	Gammaf11	0.0 in./V	0.0 mm/V
Dielectric constant (22)	Gammaf22	0.0 in./V	0.0 mm/V
Capacitance	Cef	0.0 V	0.0 V
Resistivity	Ref	0.0 Ω-in.	0.0 Ω-mm
Tensile strength	SfT	1.0E7	6895×10^6 Pa
Compressive strength	SfC	9.0E6 psi	6205×10^6 Pa
Shear strength	SfS	5.0E6 psi	3447×10^6 Pa
Normal damping capacity (11)	psi11f	0.03%Energy	0.03%Energy
Normal damping capacity (12)	psi22f	0.4%Energy	0.4%Energy
Shear damping capacity (12)	psi12f	0.4%Energy	0.4%Energy
Shear damping capacity (23)	psi23f	0.8%Energy	0.8%Energy
Melting temperature	TMf	6000.0 °F	3315.6 °C

TABLE 2.—CONVENTIONAL MATRIX (IMHS)
[INTERMEDIATE MODULUS 123M FOR SINGLE FIBER 3–D STRESS ANALYSIS.]

Description	Symbol	Value	Value in SI units
Weight density	Rhom	0.044 lb/in.^{3}	1.218×10^{-6} kg/mm^3
Normal modulus	Em	5.0E5	68.94 GPa
Poisson's ratio	Num	0.35 non-dim.	0.35 non-dim.
Thermal expansion coefficient	Alfa m	3.6×10^{-5} in./in./°F	6.48×10^{-5}/°C
Heat conductivity	Km	0.008681 BTU/hr/in./°F	1.803×10^{-4}W/mm/°C
Heat capacity	Cm	0.25 BTU/lb/°F	1048 J/kg/°C
Dielectric strength	Kem	0.0 V/in.	0.0 V/mm
Dielectric constant	Gammam	0.0 in./V	0.0 V/mm
Capacitance	Cem	0.0 V	0.0 V
Resistivity	Rem	0.0 Ω-in.	0.0 Ω-mm
Moisture expansion coefficient	Betam	0.0033 in./in./%Moisture	0.0033/%Moisture
Diffusivity	Dm	2.16×10^{-7} in.^{2}/hr	1.394×10^{-4} mm^2/hr
Saturation	Mm	0.0%Moisture	0.0%Moisture
Tensile strength	SmT	15000.0 psi	103.4 MPa
Compressive strength	SmC	35000.0 psi	241.3 MPa
Shear strength	SmS	13000.0 psi	89.63 MPa
Allowable tensile strain	eps mT	0.02 in./in.	0.02 mm/mm
Allowable compr. strain	eps mC	0.05 in./in.	0.05 mm/mm
Allowable shear strain	eps mS	0.035 in./in.	0.035 mm/mm
Allowable torsional strain	eps mTOR	0.035 in./in.	0.035 mm/mm
Normal damping capacity	psiNm	6.6%Energy	6.6%Energy
Shear damping capacity	psiSm	6.9%Energy	6.9%Energy
Void heat conductivity	Kv	0.225 BTU/hr/in./°F	4.673×10^{-3} W/mm/°C
Glass transition temperature	Tgdr	420.0 °F	215.6 °C
Melting temperature	TMm	600 °F	–17.78 °C

TABLE 3.—NANOFIBER REINFORCED MATRIX
(NFRM—0.01 FIBER REINFORCEMENT)

Description	Symbol	Value	Value in SI units
Weight density	Rhom	0.047 lb/in.^{3}	1.301×10^{-6} kg/mm^3
Normal modulus	Em	6.774×10^7 psi	467.1 GPa
Poisson's ratio	Num	0.3323 non-dim.	0.3323 non-dim
Thermal expansion coefficient	Alfa m	5.6×10^{-9} in./in./°F	10.08×10^{-9}/°C
Heat conductivity	Km	444.0 BTU/hr/in./°F	9.221 W/mm/°C
Heat capacity	Cm	0.227 BTU/lb/°F	951.1 J/kg/°C
Dielectric strength	Kem	0.0 V/in.	0.0 V/mm.
Dielectric constant	Gammam	0.0 in./V	0.0 V/mm.
Capacitance	Cem	0.0 V	0.0 V
Resistivity	Rem	0.0 Ω-in.	0.0 Ω-mm.
Moisture expansion coefficient	Betam	5.5×10^{-11} in./in./%Moisture	5.5×10^{-11}/%Moisture
Diffusivity	Dm	5.4×10^{-11} in.^{2}/hr	3.484×10^{-8} mm^2/hr
Saturation	Mm	0.0%Moisture	0.0 %Moisture
Tensile strength	SmT	800000.0 psi	5.516 GPa
Compressive strength	SmC	600000.0 psi	4.137 GPa
Shear strength	SmS	400000.0 psi	2.758 GPa
Allowable tensile strain	eps mT	0.0070 in./in.	0.0070 mm/mm
Allowable compr. strain	eps mC	0.0060 in./in.	0.0060 mm/mm
Allowable shear strain	eps mS	0.0040 in./in.	0.0040 mm/mm
Allowable torsional strain	eps mTOR	0.0040 in./in.	0.0040 mm/mm
Normal damping capacity	psiNm	0.4%Energy	0.4%Energy
Shear damping capacity	psiSm	0.4%Energy	0.4%Energy
Void heat conductivity	Kv	0.225 BTU/hr/in./°F	4.673×10^{-3} W/mm/°C
Glass transition temperature	Tgdr	420.0 °F	215.6 °C
Melting temperature	TMm	550.0 °F	287.8 °C

TABLE 4.—CONVENTIONAL FIBER (AS00)

Description	Symbol	Value	Value in SI units
Number of fibers per end	Nf	10000.0	10000.0
Filament equivalent diameter	df	3.0×10^{-4} in.	76.2×10^{-4} mm
Weight density	Rhof	0.063 lb/in.^{3}	1.744×10^{-6} kg/mm^3
Normal moduli (11)	Ef11	3.2×10^{7} psi	22.06×10^{10} Pa
Normal moduli (22)	Ef22	2000000.0 psi	13.79 GPa
Poisson's ratio (12)	Nuf12	0.2 non-dim.	0.2 non-dim.
Poisson's ratio (23)	Nuf23	0.25 non-dim.	0.25 non-dim.
Shear moduli (12)	Gf12	2000000.0 psi	13.79 GPa
Shear moduli (23)	Gf23	1000000.0 psi	6.895 GPa
Thermal expansion coefficient (11)	Alfaf11	5.5×10^{-7} in./in./°F	9.9×10^{-7}/°C
Thermal expansion coefficient (22)	Alfaf22	5.5×10^{-4} in./in./°F	9.9×10^{-4}/°C
Heat conductivity (11)	Kf11	4.03 BTU/hr/in./°F	0.08370 W/mm/°C
Heat conductivity (12)	Kf12	0.403 BTU/hr/in./°F	0.008370 W/mm/°C
Heat capacity	Cf	0.17 BTU/lb/°F	712.3 J/kg/°C
Dielectric strength (11)	Kef11	0.0 V/in.	0.0 V/mm
Dielectric strength (22)	Kef22	0.0 V/in.	0.0 V/mm
Dielectric constant (11)	Gammaf11	0.0 in./V	0.0 mm/V
Dielectric constant (22)	Gammaf22	0.0 in./V	0.0 mm/V
Capacitance	Cef	0.0 V	0.0 V
Resistivity	Ref	0.0 Ω-in.	0.0 Ω-mm
Tensile strength	SfT	400000.0 psi	2.758 GPa
Compressive strength	SfC	350000.0 psi	2.413 GPa
Shear strength	SfS	250000.0 psi	1.724 GPa
Normal damping capacity (11)	psi11f	0.05%Energy	0.05%Energy
Normal damping capacity (12)	psi22f	0.25%Energy	0.25%Energy
Shear damping capacity (12)	psi12f	0.35%Energy	0.35%Energy
Shear damping capacity (23)	psi23f	0.5%Energy	0.5%Energy
Melting temperature	TMf	6000.0 °F	3315.6 °C

TABLE 5.—BENDING RIGIDITIES OF UNIDIRECTIONAL COMPOSITE FOR BUCKLING VIBRATION FREQUENCIES ANALYSIS

θ	D_{11}	D_{12}	D_{13}	D_{22}	D_{23}	D_{33}	Comment
0	3.87 + 6	5.41 + 4	0	2.14 + 5	0	2.10 + 5	With NFRM; $k_f = 0.01$
0	1.62 + 6	2.60 + 4	0	9.98 + 4	0	5.19 + 4	Without NFRM
kPa	27.10 + 6	37.33 + 4	0	14.94 + 5	0	14.66 + 5	With NFRM; $k_f = 0.01$
kPa	11.31 + 6	18.15 + 5	0	69.60 + 4	0	36.23 + 4	Without NFRM

TABLE 6.—BUCKLING FACTOR RESULTS ON ANISOTROPIC COMPOSITE PLATES WITH CONVENTIONAL MATRIX

Load conditions in vibration frequencies			
√	0	0	–1793
0	√	0	–529
0	0	√	–1023
√	√	0	–422
√	0	√	–708
0	√	√	–383
√	√	√	–323

TABLE 7.—BUCKLING FACTOR RESULTS OF ANISOTROPIC COMPOSITE PLATES WITH NFRM

Load conditions in vibration frequencies			
√	0	0	–3673
0	√	0	–1097
0	0	√	–2220
√	√	0	–875
√	0	√	–1523
0	√	√	–808
√	√	√	–680

TABLE 8.—VIBRATION FREQUENCIES OF ANISOTROPIC COMPOSITE PLATES WITH NFRM AND WITH CONVENTIONAL MATRIX (CM) AND COMBINED LOADING

Load conditions and frequency factor, Hz				
Combined loading			NFRM	CM
√	0	0	2005	1390
0	√	0	1818	1270
0	0	√	2245	1576
√	√	0	1819	1270
√	0	√	2122	1490
0	√	√	1909	1339
√	√	√	1898	1331

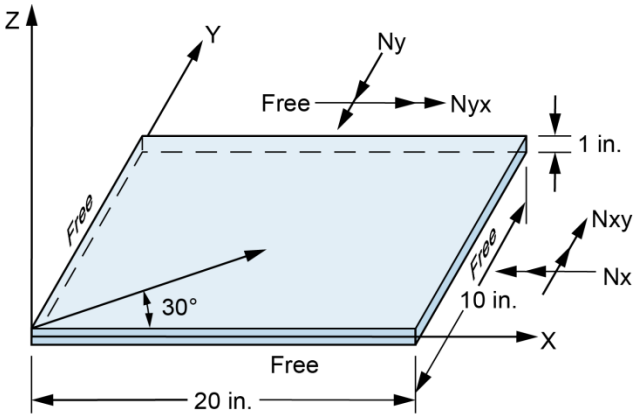

Figure 1.—Anisotropic plate schematic.

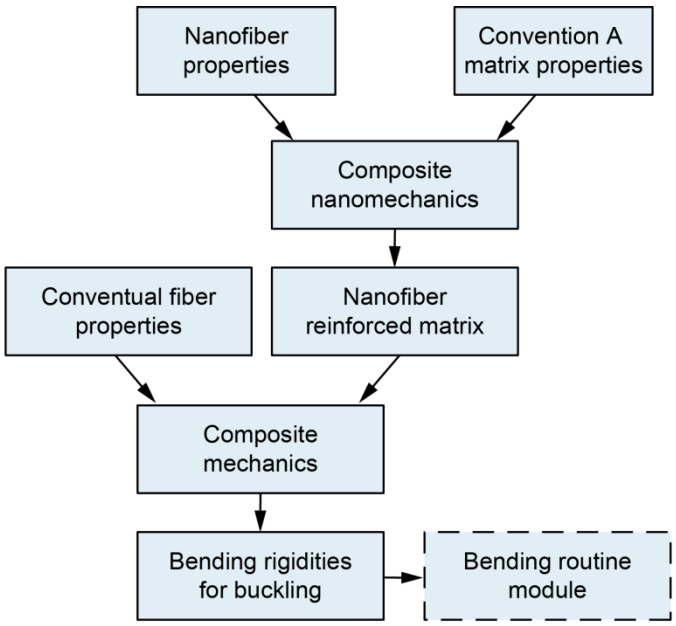

Figure 2.—Simulation of nanofiber reinforced matrix schematic.

Buckling Mode Shapes

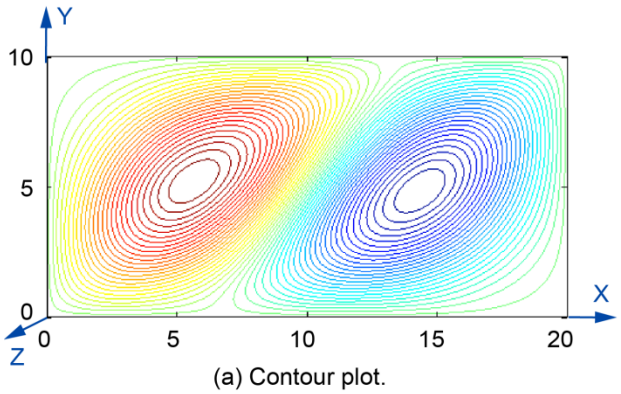

(a) Contour plot.

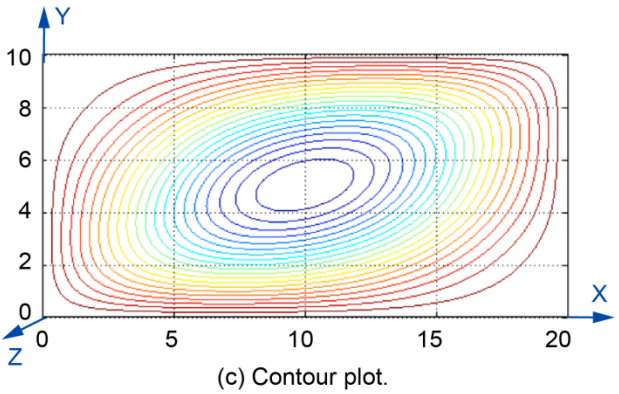

(c) Contour plot.

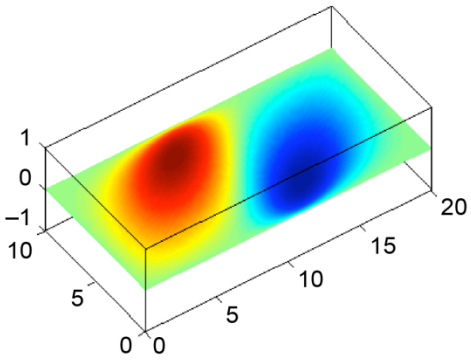

(b) Three–dimensional display.

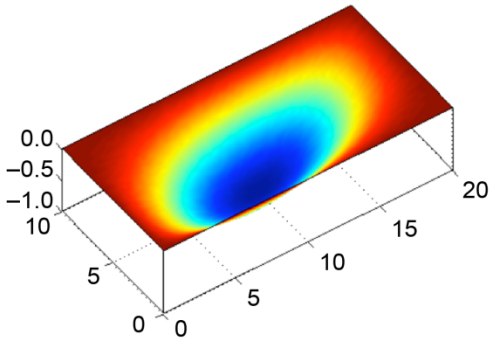

(d) Three–dimensional display.

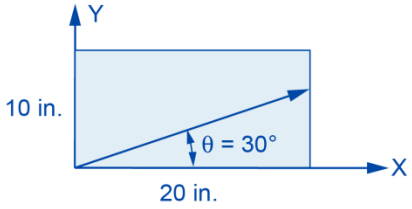

(e) Buckling information.

Ncr = critical buckling factor = 3673
Buckling load = Ncr [–100, 0, 0]
Applied load = 0.6 Ncr [–100, 0, 0]
Load axes = 30° to material axis;
First natural frequency = 2005 Hz

(f) Frequency information.

Figure 3.—Buckling factor and first frequency vibration mode.

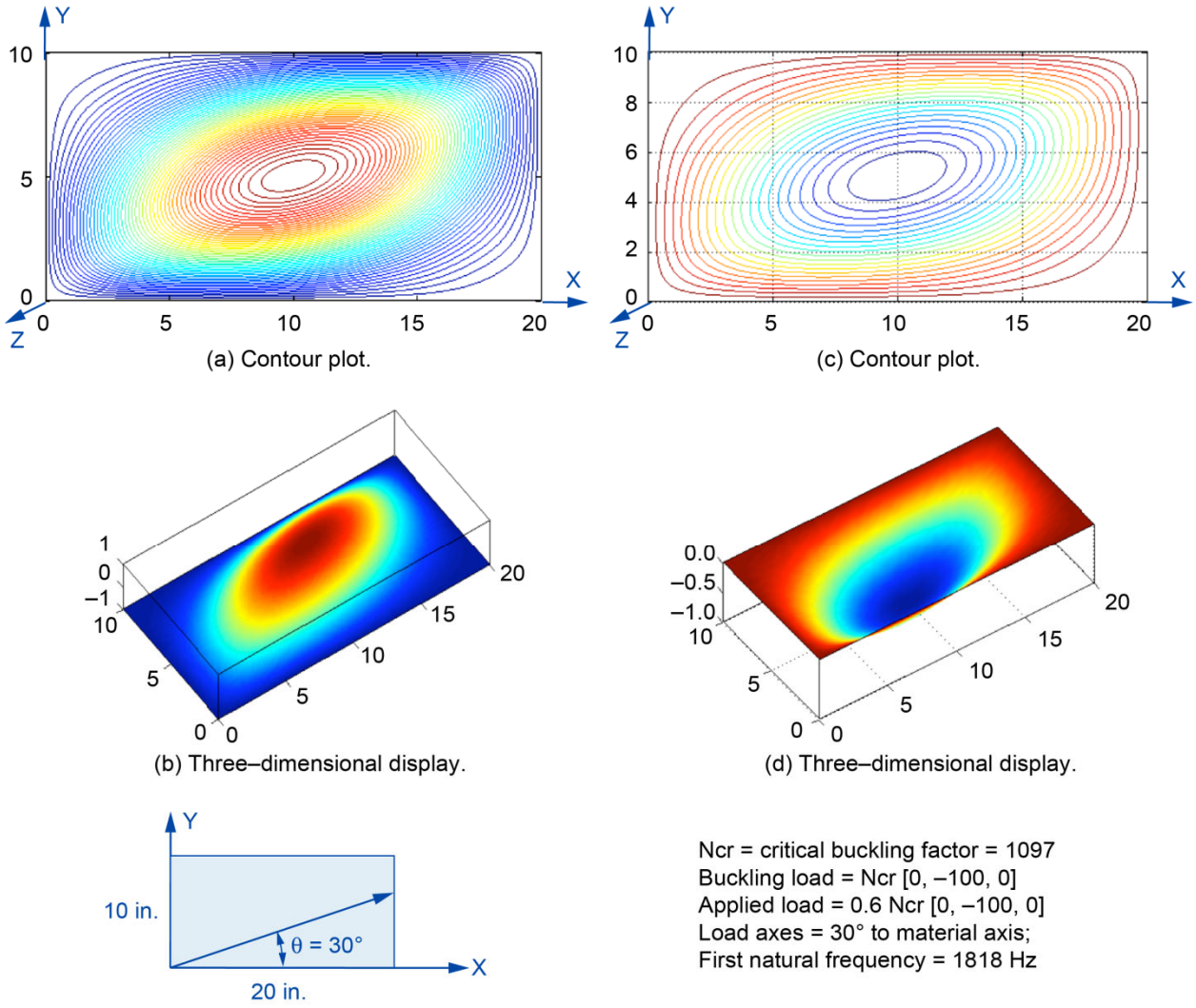

Figure 4.—Buckling factor and first frequency vibration mode.

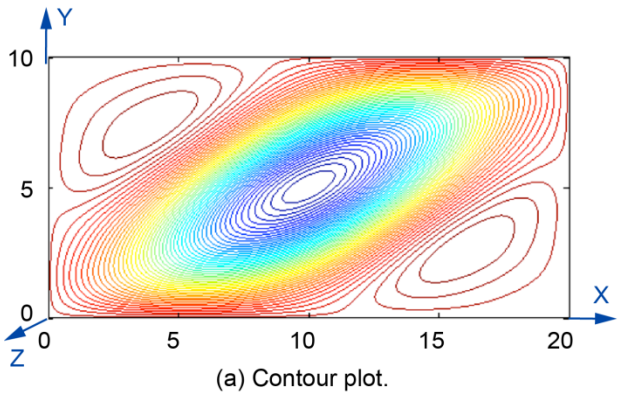

(a) Contour plot.

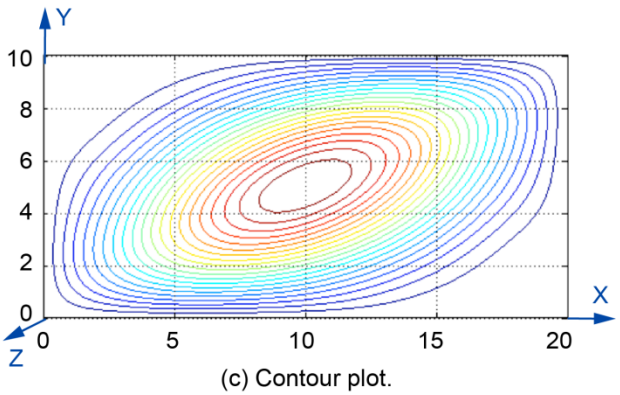

(c) Contour plot.

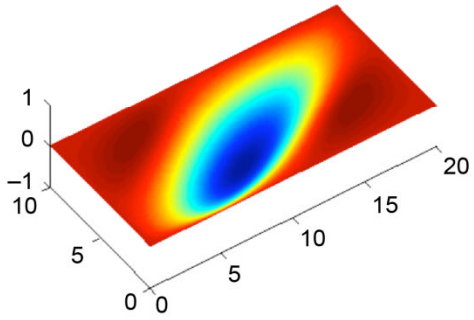

(b) Three–dimensional display.

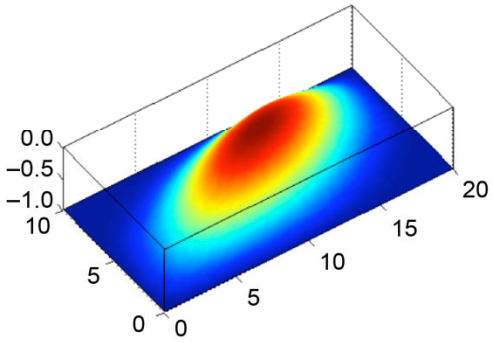

(d) Three–dimensional display.

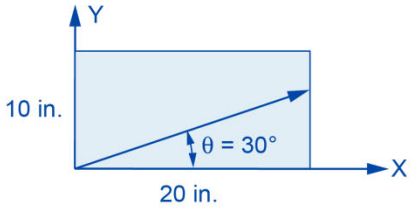

Ncr = critical buckling factor = 2220
Buckling load = Ncr [–1, –1, –100]
Applied load = 0.6 Ncr [–1, –1, –100]
Load axes = 30° to material axis;
First natural frequency = 2245 Hz

(e) Buckling information.

Figure 5.—Buckling factor and first frequency vibration mode.

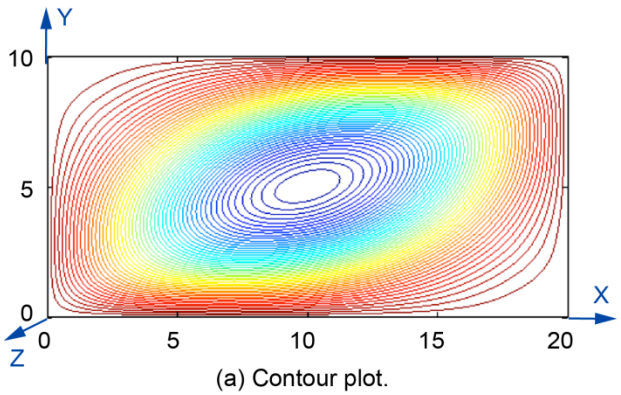

(a) Contour plot.

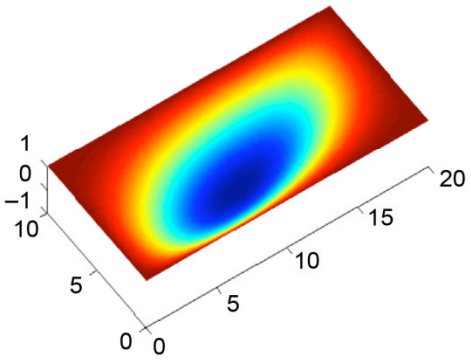

(b) Three–dimensional display.

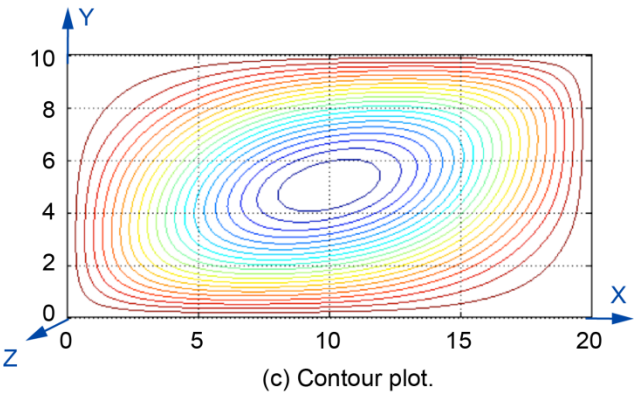

(c) Contour plot.

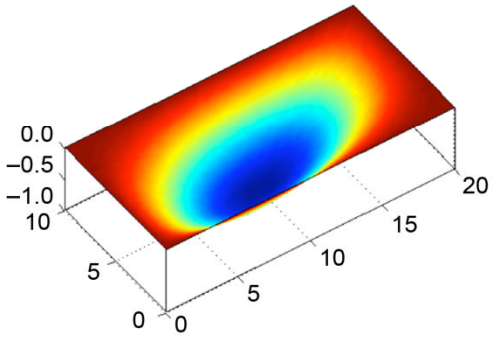

(d) Three–dimensional display.

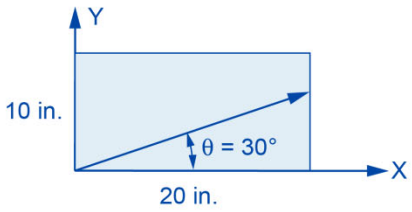

Ncr = critical buckling factor = 875
Buckling load = Ncr [–100, –100, 0]
Applied load = 0.6 Ncr [–100, –100, 0]
Load axes = 30° to material axis;
First natural frequency = 1819 Hz

(e) Buckling information.

Figure 6.—Buckling factor and first frequency vibration mode.

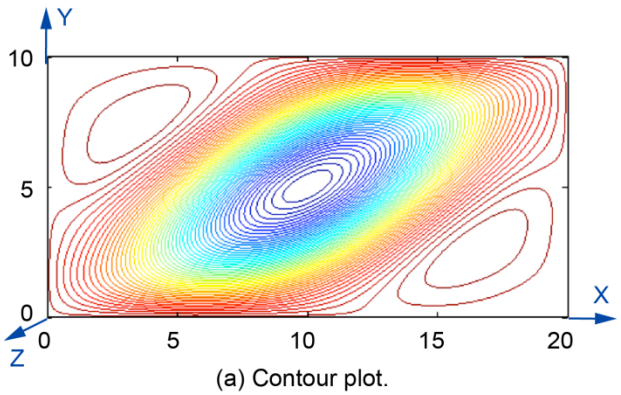

(a) Contour plot.

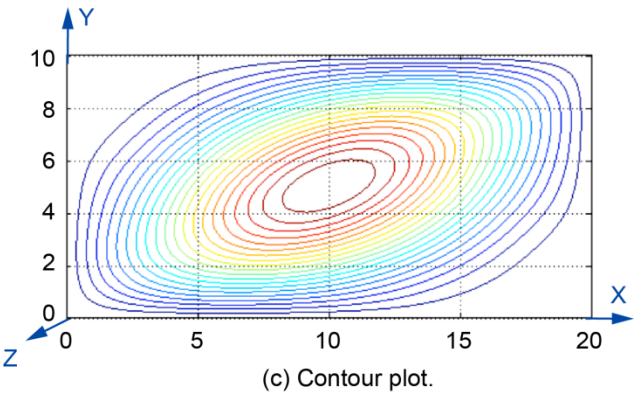

(c) Contour plot.

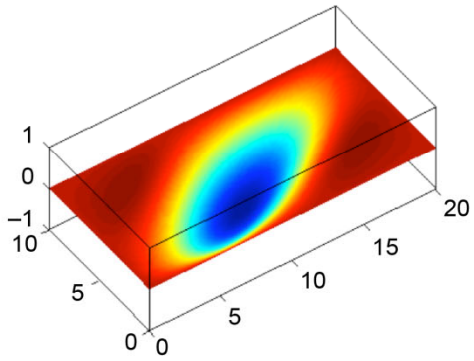

(b) Three–dimensional display.

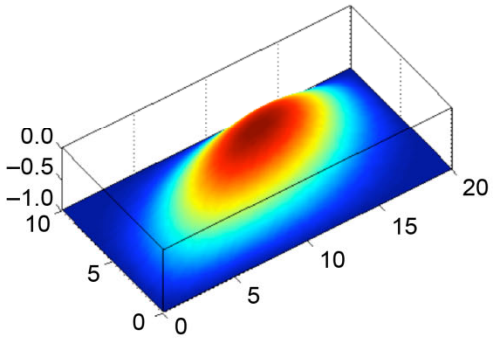

(d) Three–dimensional display.

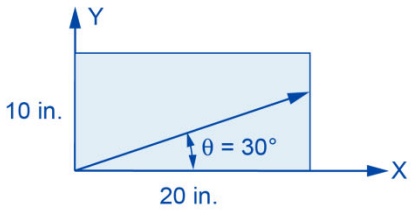

Ncr = critical buckling factor = 1520
Buckling load = Ncr [–100, 0, –100]
Applied load = 0.6 Ncr [–100, 0, –100]
Load axes = 30° to material axis;
First natural frequency = 2121 Hz

(e) Buckling information.

Figure 7.—Buckling factor and first frequency vibration mode.

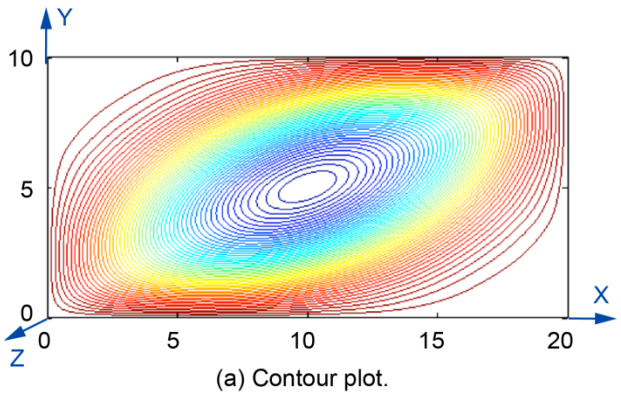

(a) Contour plot.

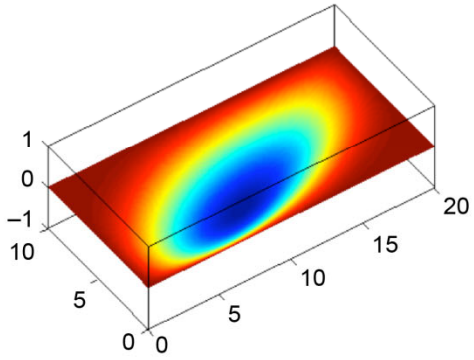

(b) Three–dimensional display.

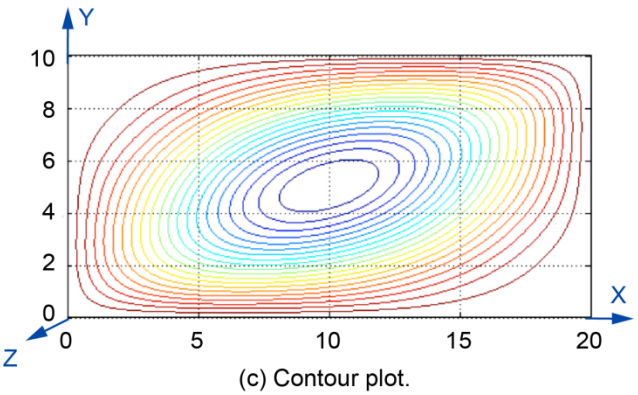

(c) Contour plot.

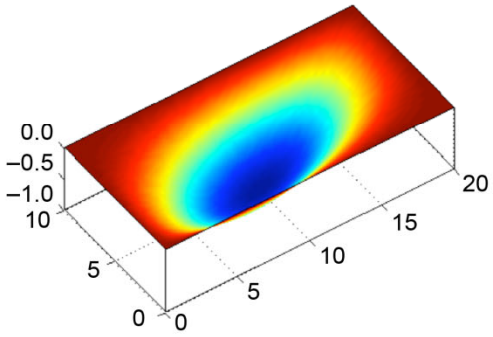

(d) Three–dimensional display.

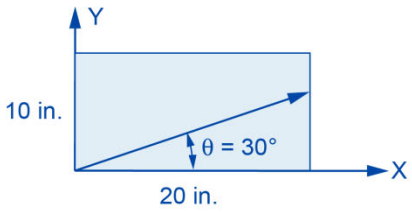

Ncr = critical buckling factor = 808
Buckling load = Ncr [0, –100, –100]
Applied load = 0.6 Ncr [0, –100, –100]
Load axes = 30° to material axis;
First natural frequency = 1909 Hz

(e) Buckling information.

Figure 8.—Buckling factor and first frequency vibration mode.

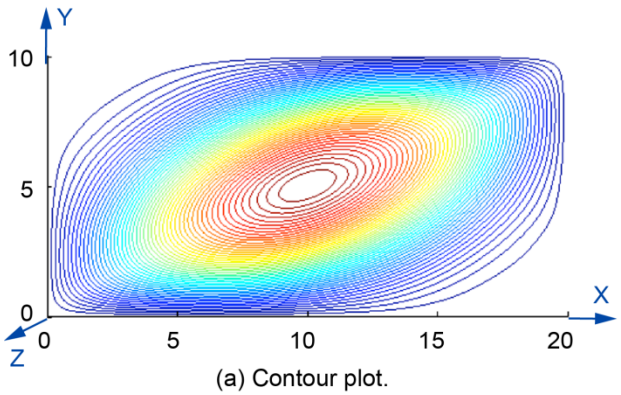

(a) Contour plot.

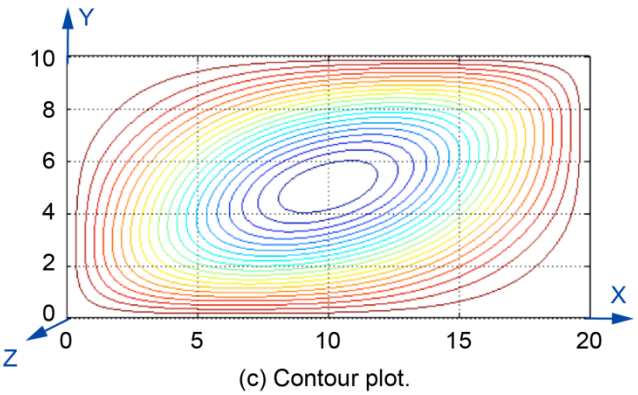

(c) Contour plot.

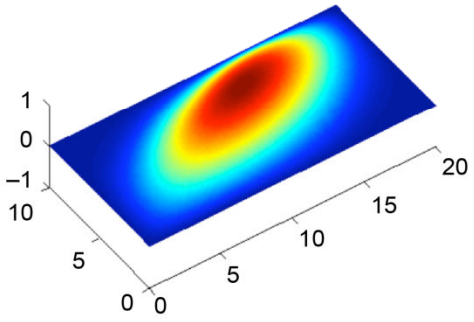

(b) Three–dimensional display.

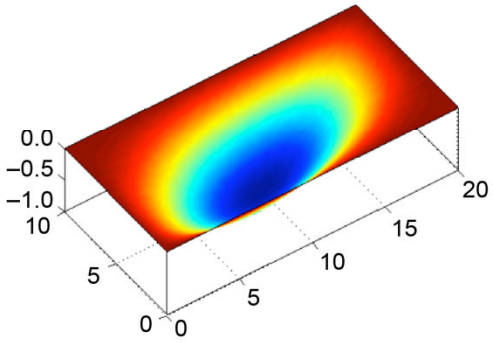

(d) Three–dimensional display.

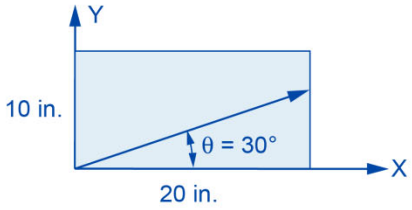

Ncr = critical buckling factor = 680
Buckling load = Ncr [–100, –100, –100]
Applied load = 0.6 Ncr [–100, –100, –100]
Load axes = 30° to material axis;
First natural frequency = 1898 Hz

(e) Buckling information.

Figure 9.—Buckling factor and first frequency vibration mode.

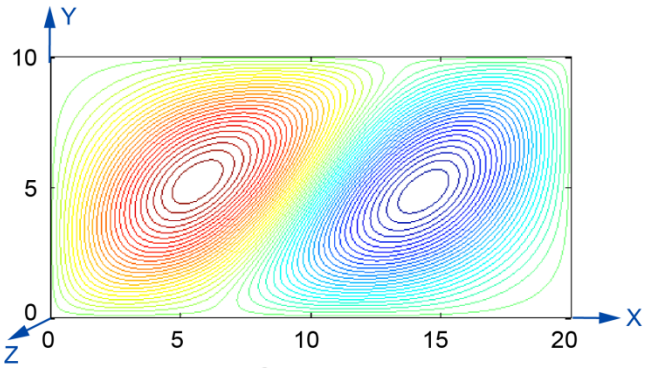

(a) Contour plot.

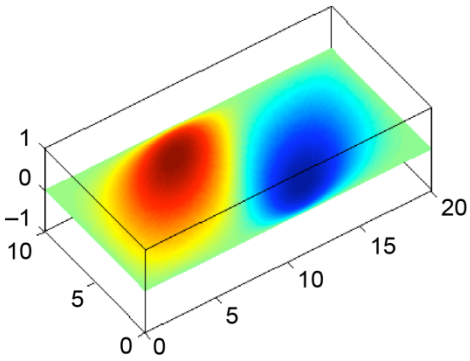

(b) Three–dimensional display.

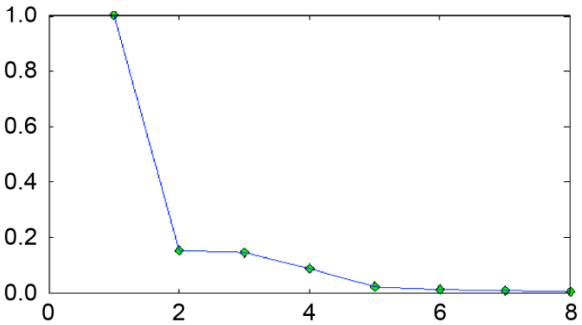

(c) Convergence iteration

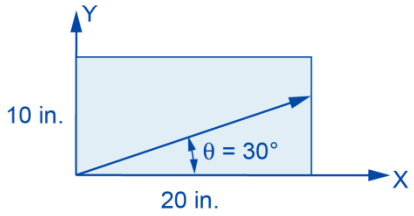

ρ = [–100, 0, 0]
Load axes = 30° to material
Axis; Ncr = 3673

(d) Buckling information.

Figure 10.—Buckling mode shapes and convergence of fiber composites anisotropic plates with 0.01 nanofiber reinforced matrix loaded in the structural X–axis.

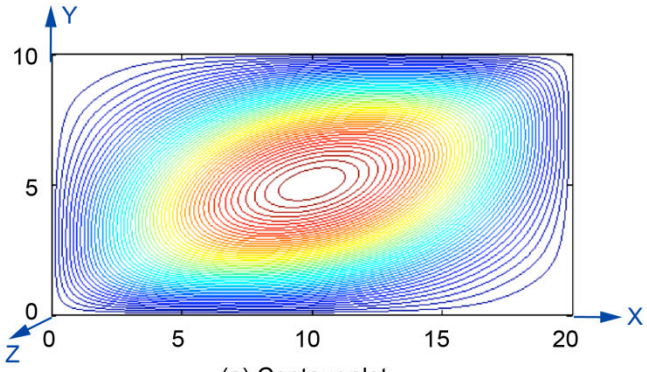

(a) Contour plot.

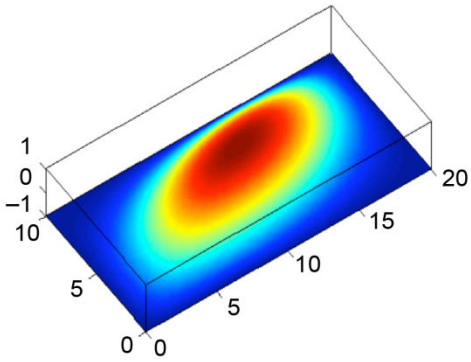

(b) Three–dimensional display.

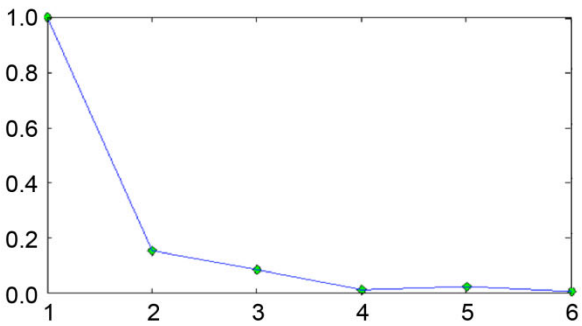

(c) Convergence iteration

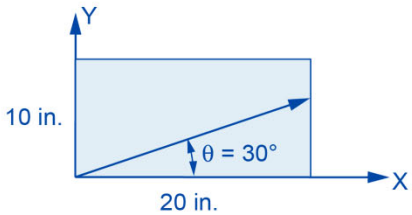

ρ = [0, –100, 0]
Load axes = 30° to material
Axis; Ncr = 1097

(d) Buckling information.

Figure 11.—Buckling mode shapes and convergence of fiber composites anisotropic plates with 0.01 nanofiber reinforced matrix loaded in the structural Y–axis.

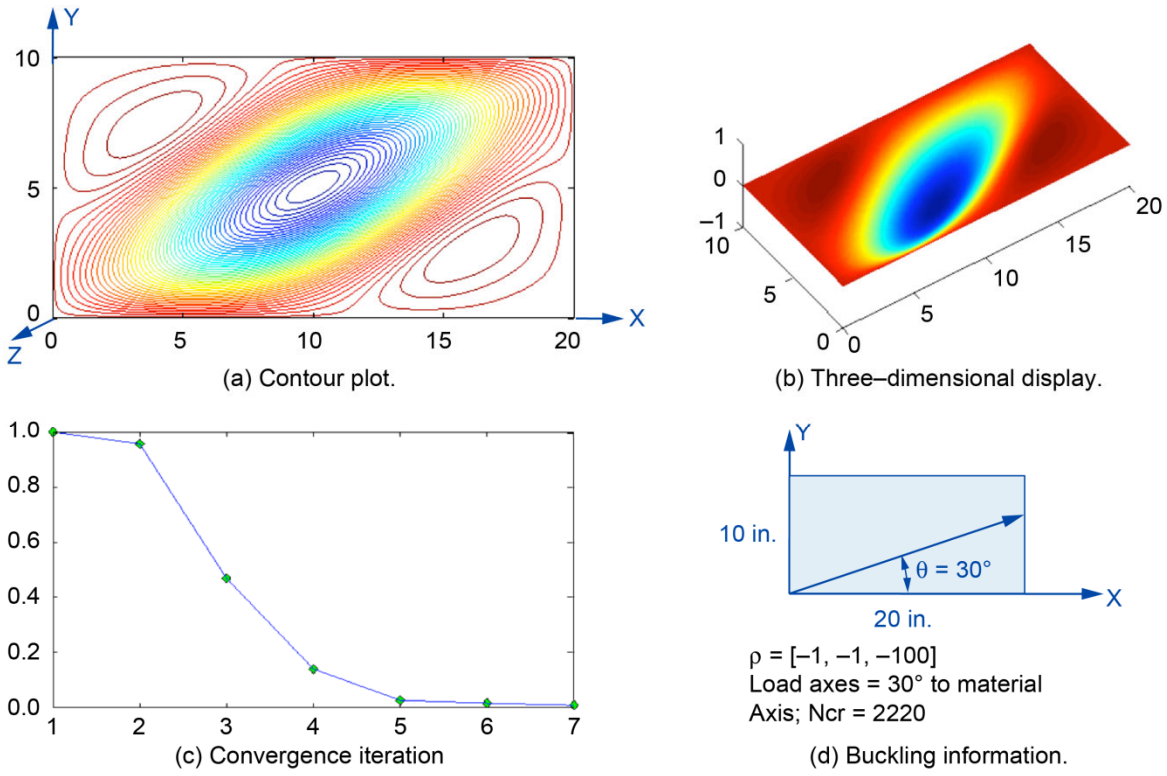

Figure 12.—Buckling mode shapes and convergence of fiber composites anisotropic plates with 0.01 nanofiber reinforced matrix loaded in the structural XY–axis.

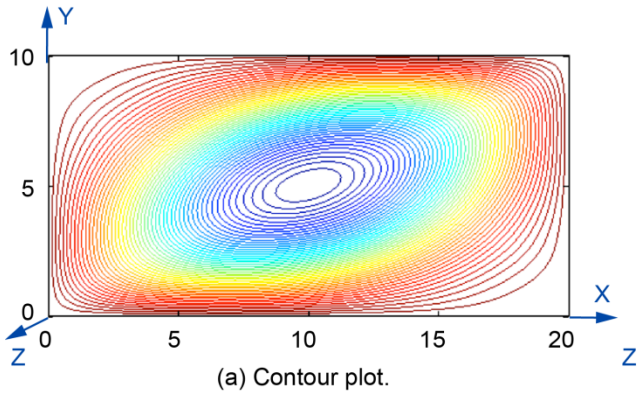

(a) Contour plot.

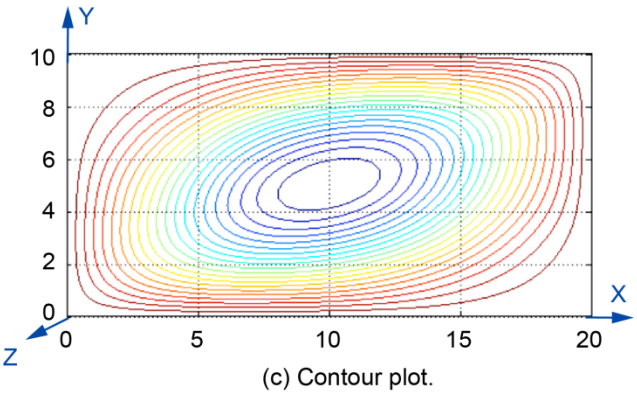

(c) Contour plot.

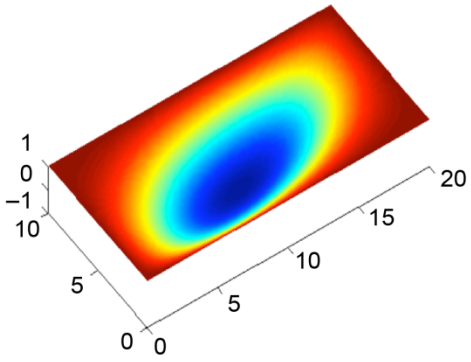

(b) Three–dimensional display.

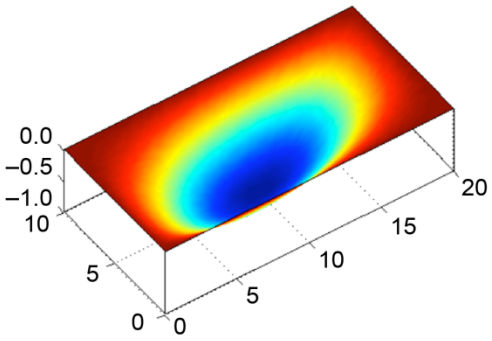

(d) Three–dimensional display.

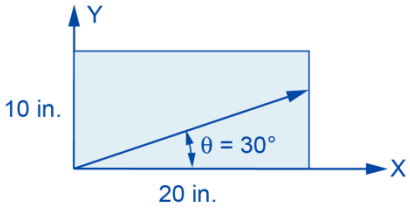

Ncr = critical buckling factor = 875
Buckling load = Ncr [–100, –100, 0]
Applied load = 0.6 Ncr [–100, –100, 0]
Load axes = 30° to material axis;
First natural frequency = 1819 Hz

(e) Buckling information.

Figure 13.—Buckling factor and first frequency vibration mode.

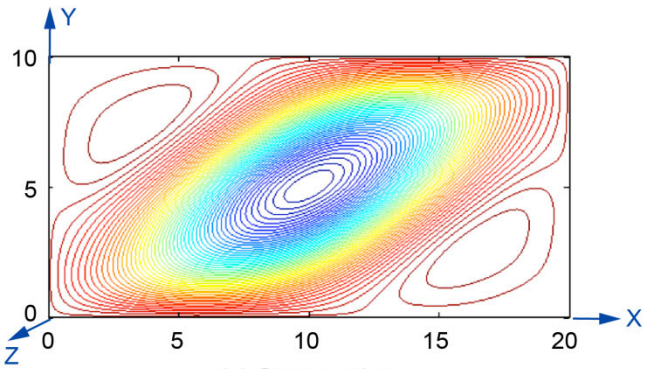

(a) Contour plot.

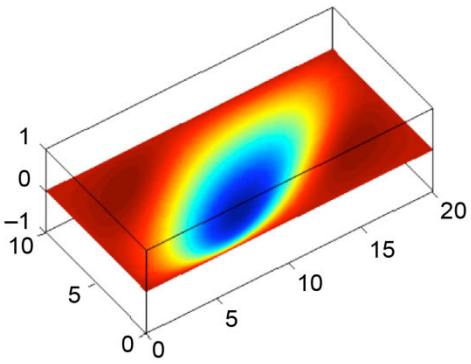

(b) Three–dimensional display.

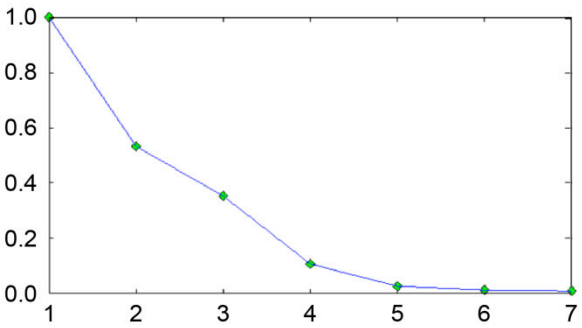

(c) Convergence iteration

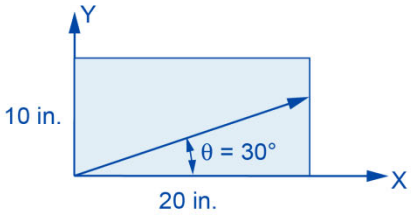

ρ = [–100, 0, –100]
Load axes = 30° to material
Axis; Ncr = 2220

(d) Buckling information.

Figure 14.—Buckling mode shapes and convergence of fiber composites anisotropic plates with 0.01 nanofiber reinforced matrix loaded in the structural X and XY–axis.

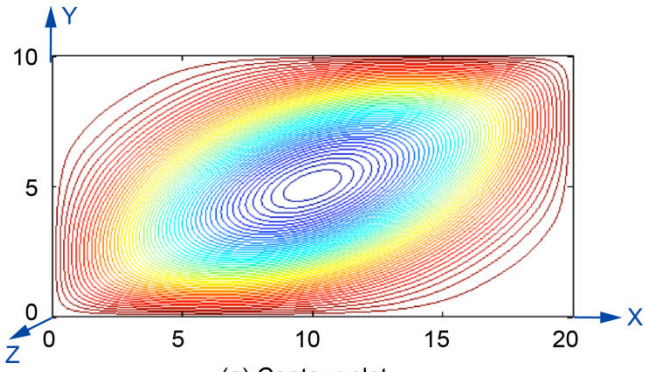

(a) Contour plot.

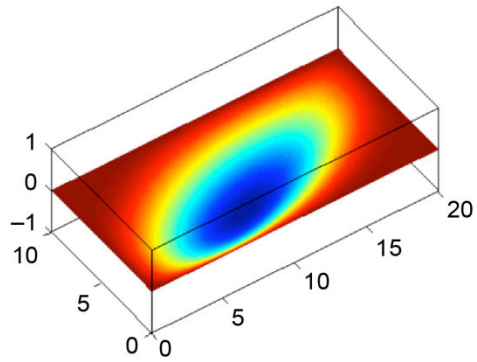

(b) Three–dimensional display.

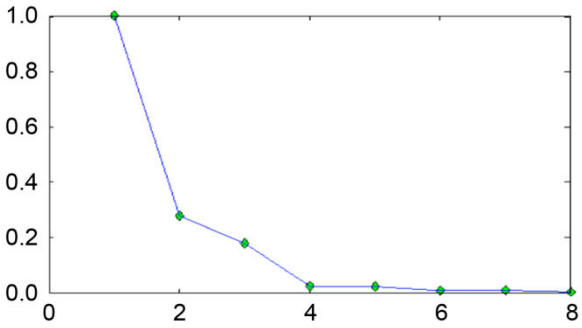

(c) Convergence iteration

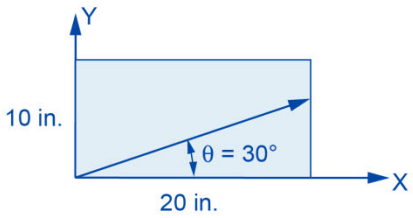

ρ = [0, –100, –100]
Load axes = 30° to material
Axis; Ncr = 808

(d) Buckling information.

Figure 15.—Buckling mode shapes and convergence of fiber composites anisotropic plates with 0.01 nanofiber reinforced matrix loaded in the structural Y and XY–axis.

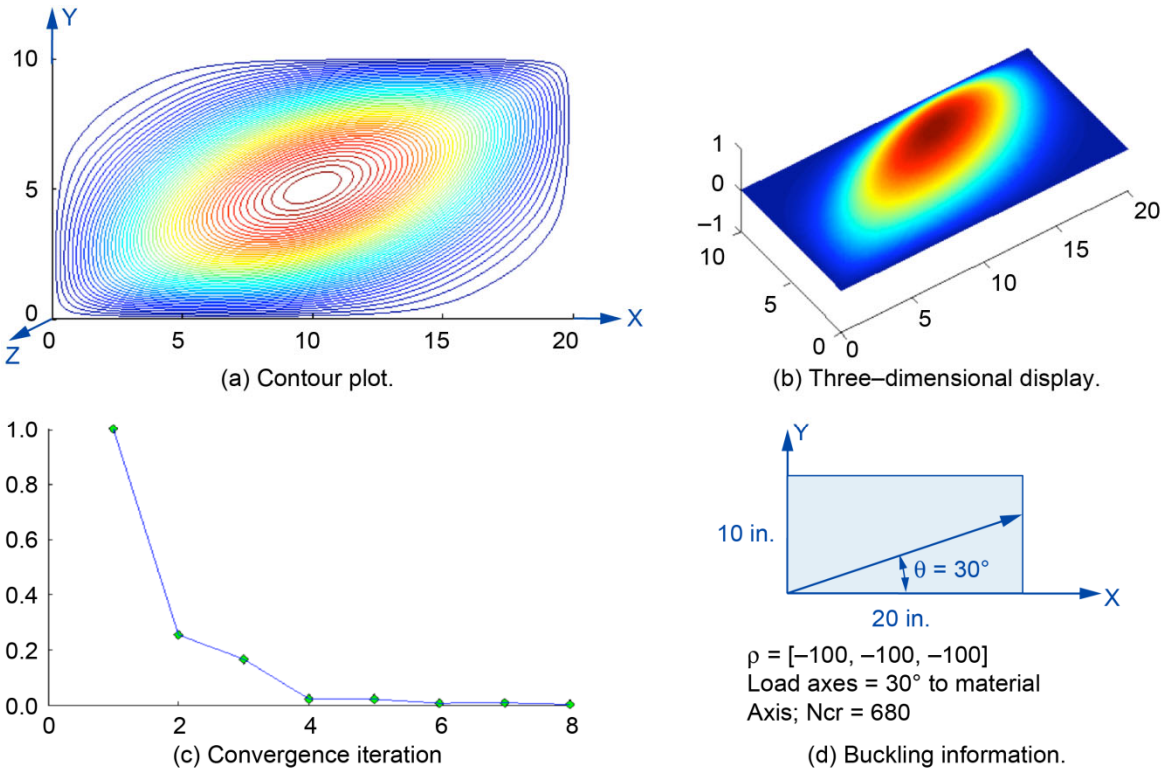

Figure 16.—Buckling mode shapes and convergence of fiber composites anisotropic plates with 0.01 nanofiber reinforced matrix loaded in the structural X and Y and XY–axis.

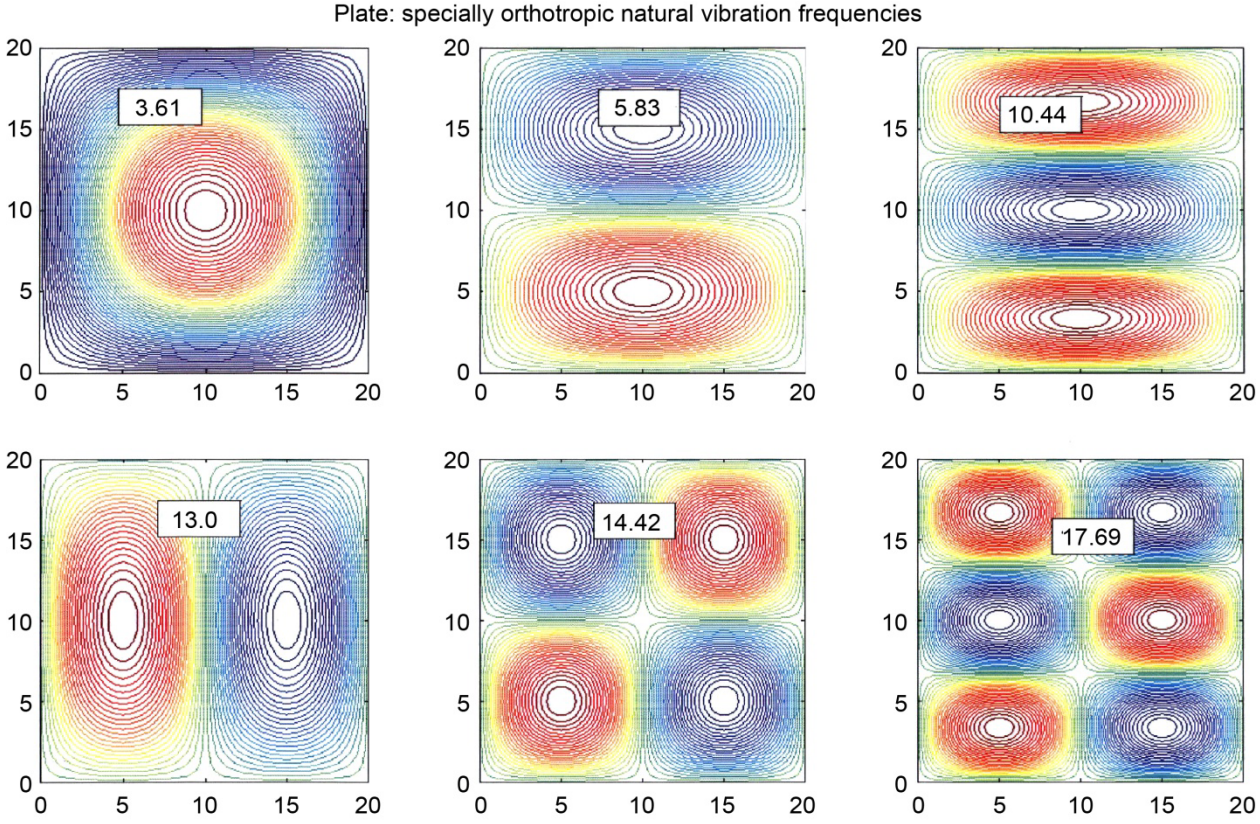

Figure 17.—First six vibration frequencies mode shapes of a square plate.

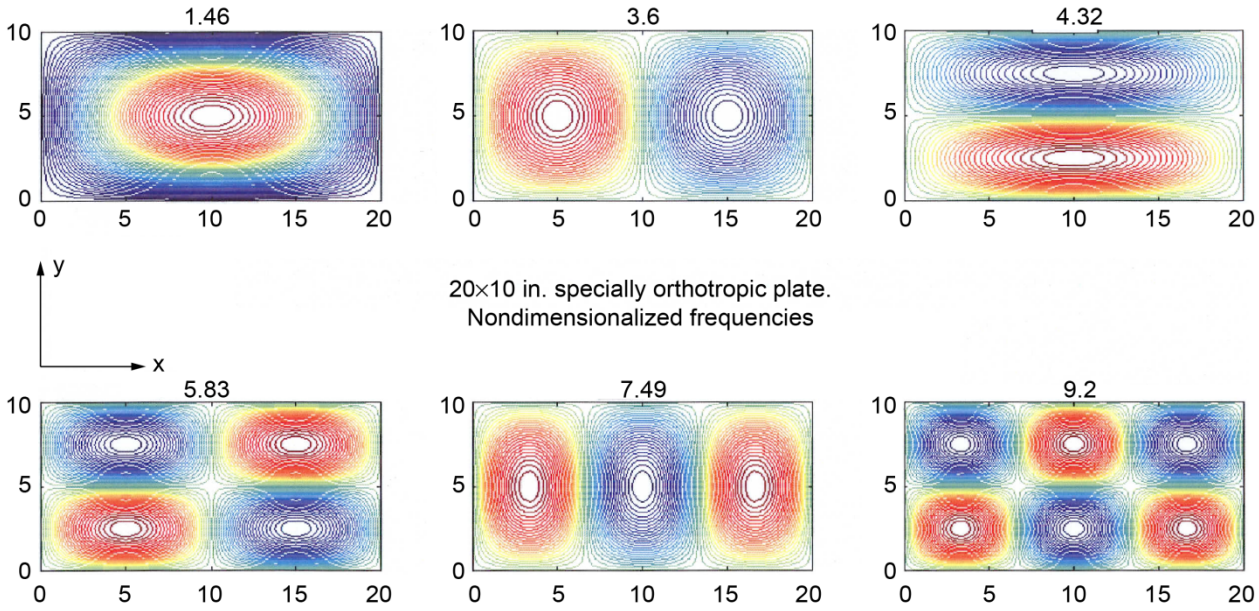

Figure 18.—First six vibration mode shapes of a rectangular plate.

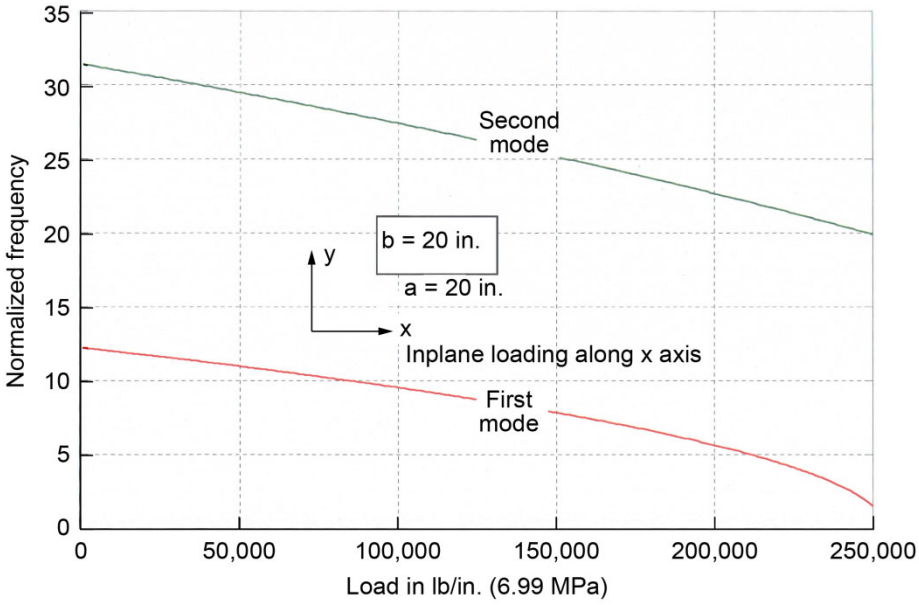

Figure 19.—Load effects on frequency.

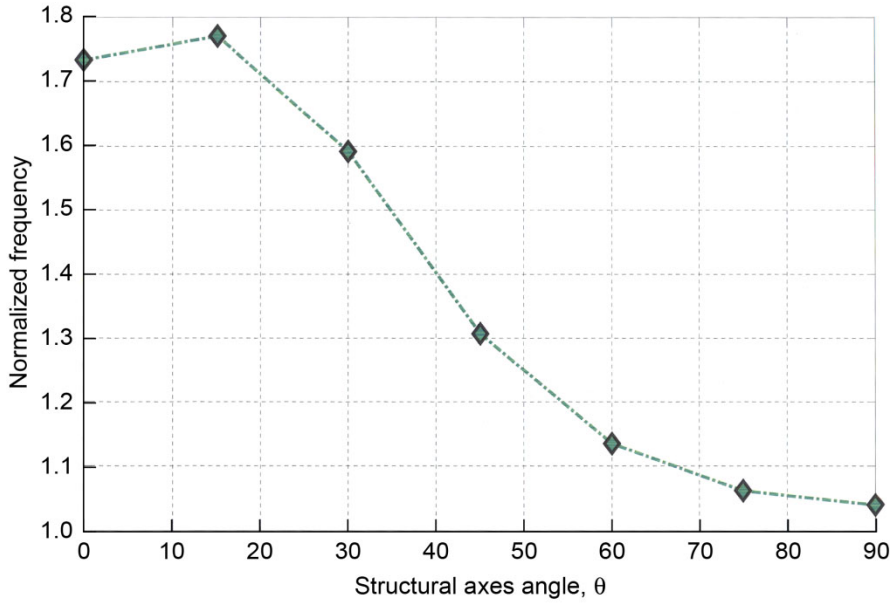

Figure 20.—Orientation angle effects on frequency.

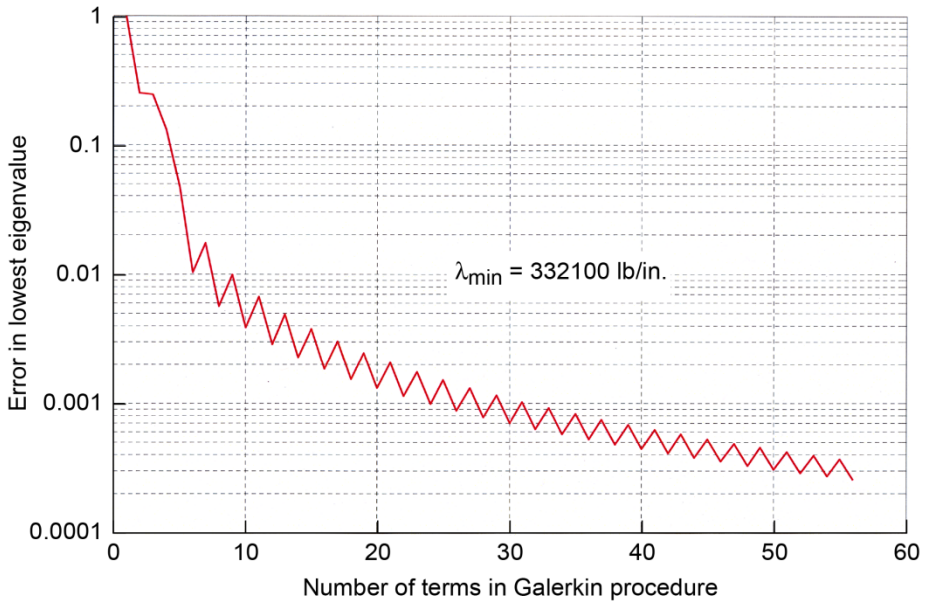

Figure 21.—Eigenvalue convergence versus number of terms in the Galerkin procedure.

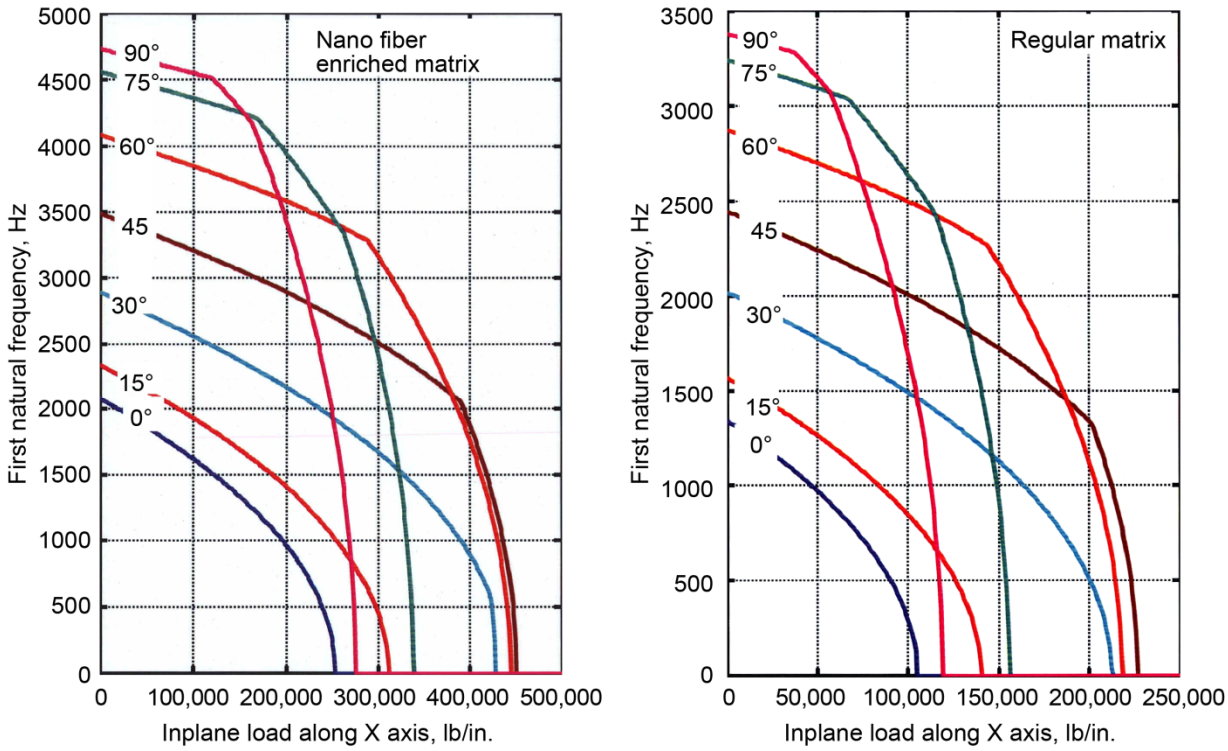

Figure 22.—Increasing load effects on anisotropic frequencies.

REPORT DOCUMENTATION PAGE	Form Approved OMB No. 0704-0188

1. REPORT DATE *(DD-MM-YYYY)*	2. REPORT TYPE	3. DATES COVERED *(From - To)*
01-12-2011	Technical Memorandum	

4. TITLE AND SUBTITLE
Buckling and Vibration of Fiber Reinforced Composite Plates With Nanofiber Reinforced Matrices

5a. CONTRACT NUMBER

5b. GRANT NUMBER

5c. PROGRAM ELEMENT NUMBER

6. AUTHOR(S)
Chamis, Christos, C.; Murthy, Pappu, L.N.

5d. PROJECT NUMBER

5e. TASK NUMBER

5f. WORK UNIT NUMBER
WBS 561581.02.08.03.13.05

7. PERFORMING ORGANIZATION NAME(S) AND ADDRESS(ES)
National Aeronautics and Space Administration
John H. Glenn Research Center at Lewis Field
Cleveland, Ohio 44135-3191

8. PERFORMING ORGANIZATION REPORT NUMBER
E-18037

9. SPONSORING/MONITORING AGENCY NAME(S) AND ADDRESS(ES)
National Aeronautics and Space Administration
Washington, DC 20546-0001

10. SPONSORING/MONITOR'S ACRONYM(S)
NASA

11. SPONSORING/MONITORING REPORT NUMBER
NASA/TM-2011-217282

12. DISTRIBUTION/AVAILABILITY STATEMENT
Unclassified-Unlimited
Subject Category: 24
Available electronically at http://www.sti.nasa.gov
This publication is available from the NASA Center for AeroSpace Information, 443-757-5802

13. SUPPLEMENTARY NOTES

14. ABSTRACT
Anisotropic composite plates were evaluated with nanofiber reinforced matrices (NFRM). The nanofiber reinforcement volumes ratio in the matrix was 0.01. The plate dimensions were 20 by 10 by 1.0 in. (508 by 254 by 25.4 mm). Seven different loading condition cases were evaluated for buckling: three for uniaxial loading, three for pairs of combined loading, and one with three combined loadings. The anisotropy arose from the unidirectional plates having been at 30° from the structural axis. The anisotropy had a full 6 by 6 rigidities matrix which were satisfied and solved by a Galerkin buckling algorithm. For vibration the same conditions were used with the applied cods about a small fraction of the buckling loads. The buckling and vibration results showed that the NFRM plates buckled at about twice those with conventional matrix.

15. SUBJECT TERMS
30° loading axis; 0.1 nano fibers; Combined loads; Unidirectional plates

16. SECURITY CLASSIFICATION OF:			17. LIMITATION OF ABSTRACT	18. NUMBER OF PAGES	19a. NAME OF RESPONSIBLE PERSON
a. REPORT	b. ABSTRACT	c. THIS PAGE			STI Help Desk (email:help@sti.nasa.gov)
U	U	U	UU	31	19b. TELEPHONE NUMBER *(include area code)* 443-757-5802